Environmental hazards of pyroclastic flows determined by numerical models

Greg A. Valentine
Mail Stop F665, Geoanalysis Group ESS-5, Los Alamos National Laboratory
Los Alamos, New Mexico 87545
Kenneth H. Wohletz
Mail Stop D462, Geology/Geochemistry Group ESS-1, Los Alamos National Laboratory
Los Alamos, New Mexico 87545

ABSTRACT

Numerical solutions of the compressible, multiphase Navier-Stokes equations are applied to conditions appropriate for the development of pyroclastic flows from collapsing Plinian eruption columns. Temporal and spatial variations in horizontal velocity, dynamic pressure, solid volume fraction, and temperature are analyzed for three experiments that model variations in behavior due to differing eruption conditions. Pyroclastic flows display a complex evolution with time and runout distance from the vent. Evolution of flow parameters is most generally manifested by alternating periods of erosion and deposition. Velocities of flow heads decrease and solid concentrations in the flow heads increase with distance from vent. Application of numerical modeling to such phenomena can help in assessing volcanic hazards and pyroclastic transport processes.

INTRODUCTION

Studies of explosive volcanic hazards have advanced rapidly over the past 20 years, as quantitative data for recent and historic eruptions have accumulated and theoretical treatments of the eruptions have been developed. In particular, much work has centered on the inverse problem of determining eruption dynamics and hazards from the characteristics of Plinian fallout deposits (Carey and Sparks, 1986; Carey and Sigurdsson, 1985, 1986, 1987; Sigurdsson et al., 1985). Successful models of fallout deposits have been obtained largely because the depositional mechanism is mathematically tractable when certain restricting simplifications are made (e.g., Wilson, 1976; Wilson et al., 1978, 1980; Sparks and Wilson, 1982; Sparks, 1986; Carey and Sparks, 1986; Wilson and Walker, 1987; Woods, 1988).

Some of the most devastating events of explosive eruptions are those caused by lateral flow of gas-particle mixtures away from the volcanoes in pyroclastic flows and surges (e.g., Kieffer, 1981; Sigurdsson et al., 1987). Pyroclastic flows involve a wide range of dynamical processes including, but not limited to, the following: turbulence, compressible flow (Kieffer, 1981), blast phenomena (Wohletz et al., 1984), fluidization (Wilson, 1980, 1984, 1985), stratified flow (Valentine, 1987), bed-load transport (Wohletz and Sheridan, 1979), and high-particle-concentration debris-flow processes (Sparks, 1976; Freundt and Schmincke, 1986; Valentine and Fisher, 1986). Pyroclastic flow hazard evaluation generally includes mapping of pyroclastic flow deposits from previous eruptions to determine hazard zones (e.g., Crandell and Hoblitt, 1986; Siebert et al., 1987), and more recently the energy-line approach, which relates pyroclastic flow runout to initial potential energy and dissipation (Sheridan, 1979; Malin and Sheridan, 1982; Beget and Limke, 1988). The above approaches provide information about the areal extent of hazardous zones; the goal of the work described here is quantification of the destructive potential *within* hazardous zones.

We present results of numerical modeling of pyroclastic flows and their implications for evaluating pyroclastic flow hazards. In this paper the term "pyroclastic flow" is used only in reference to the lateral flow of gas and tephra along the ground away from the vent where an explosive eruption is occurring; we do not distinguish among various types of pyroclastic flows and surges, which have been discussed in the volcanology literature (e.g., Valentine, 1987).

MODEL ASSUMPTIONS

Our models are based upon the premise that the dynamics of pyroclastic flows can be accurately described by the multiphase Navier-Stokes form of conservation of mass, momentum, and specific internal energy. A detailed theoretical presentation of the model is given in Valentine and Wohletz (1989). In the solution of this set of equations, we assume that the gas and solid particle phases have constant specific heats, the gas is dominantly steam and behaves as a perfect gas, and the particles are incompressible. A two-dimensional, cylindrical symmetry is chosen for the models (the symmetry axis extending upward from the center of the vent), allowing detailed computation along a radial and vertical axis from the vent. Although these models are appropriate for central-vent eruptions, the general physical processes are similar for an elongate vent (such as a caldera ring vent). Two significant limitations of our models are (1) each numerical experiment contains only one particle size, and (2) turbulence is calculated by a mixing-length approach. These limitations are discussed in detail in Valentine and Wohletz (1989).

COMPUTATIONAL APPROACH

Briefly, the governing equations of the models include eight coupled, time-dependent, nonlinear, partial differential equations that describe the conservation conditions for both the solid and the gas phases. These equations are closed with eight algebraic equations that describe the equations of state, and momentum transfer (drag) and energy exchange between the phases.

The partial differential equations are cast in finite-difference form according to the IMF (implicit multiphase flow) technique of Harlow and Amsden (1975). The flow field is calculated for a square area that is 7 km in the radial (r) direction and 7 km in the vertical (z) direction. The r-z origin corresponds to the center of the vent exit plane, and the r axis corresponds to the Earth's surface. The domain is divided into a mesh of 100×100 m squares. The Earth's surface is modeled as a free-slip reflector because boundary-layer processes occur on a scale much smaller than the computational mesh. A specified eruption discharge begins at time $t = 0$. All flow variables are computed for each cell in time steps of 0.02 s, and output is recorded at specified intervals. The time step and mesh size allow calculation for flow speeds up to 5000 m/s (determined by the Courant condition). A typical run requires about 2.5 h of Cray-1 computer time to calculate 200 s of eruption time.

The advantage of this modeling approach is that the results are simulations or experiments, the only approximations being those of the finite-difference formulation and the assumptions discussed above. In contrast

with previous work where some of the governing equations are not solved (e.g., neglect of conservation of internal energy and idealization to incompressible flow have been common approaches in the past; Sparks, 1986; Wilson, 1976), this treatment fully retains the nonlinear interactions among flow variables. Computational results are recorded graphically, producing "snapshots" of eruptions at any given time in their evolution (Valentine and Wohletz, 1989), and numerical results are tabulated to quantify spatial and temporal flow-parameter variations. In this paper we analyze variations of flow variables of three model eruptions to show lateral effects of pyroclastic flows.

RESULTS FROM NUMERICAL PYROCLASTIC FLOWS

Table 1 lists eruption conditions of experimental models 1, 2, and 3 (Figs. 1, 2, and 3, respectively). Figures 1 and 2 show results from eruptions with identical discharge properties, except for a variation in pyroclast size (diameter = 0.2 mm in Fig. 1, 2.0 cm in Fig. 2). Figure 3 gives results from an eruption with discharge similar to that deduced by Carey and Sigurdsson (1985) for the May 18, 1980, Mount St. Helens Plinian eruption.

For each model eruption, four flow parameters, including velocity, dynamic pressure, solid volume fraction, and temperature, are plotted as functions of radial distance from vent center for three times. The flow parameters were chosen to best characterize the damage potential of pyroclastic flows. Within the area where the pyroclastic flows are present, the plotted velocity is that of the particles; beyond the range of pyroclastic flows, velocity corresponds to the atmospheric wind. Positive values indicate flow away from the vent, and negative velocities are directed toward the vent. Dynamic pressure (P_{dyn}) is given by

$$P_{dyn} = (\theta\rho_s + [1-\theta]\rho_g)\, u^2, \quad (1)$$

where θ is the volume fraction of solids, ρ_s is the material density of the particles, ρ_g is the gas density, and u is the horizontal velocity (of particles within the pyroclastic flows and atmosphere beyond them). Dynamic pressure can be thought of as "wind pressure." Because we use the horizontal component of velocity, P_{dyn} decreases to small values where flows are predominantly vertical. Near the vent, vertical flow occurs where the collapsing fountain hits the ground. Dynamic pressure plots can be somewhat misleading at that point because lateral velocity vanishes (producing $P_{dyn} = 0$ by equation 1), but that location is by no means a safe place because the downward-directed velocity is large. The third variable shown is θ, and the fourth is temperature of the pyroclasts.

TABLE 1. VENT EXIT CONDITIONS FOR MODEL PYROCLASTIC FLOWS

Model	Exit velocity (m/s)	Exit pressure (Pa)	Vent radius (m)	θ*	Particle diameter (mm)	Mass discharge (kg/s)
1	300	10^5	200	10^{-2}	0.2	9.0×10^8
2	300	10^5	200	10^{-2}	20.0	9.0×10^8
3	205	10^5	100	3.1×10^{-3}	0.2	4.8×10^7

Note: Exit temperature = 1200 K and particle material density = 2400 kg/m^3 for all model eruptions.
*θ = volume fraction of solid phase (ash).

Figure 1 illustrates development of a pyroclastic flow produced by an eruption fountain that reaches an elevation of about 4 km before collapsing downward to hit the ground at about 2.9 km from vent center, at which point the horizontal components of velocity and dynamic pressure are zero. At t = 109 s, the collapsing flow has just impinged upon the ground, resulting in pyroclastic flows moving radially outward to about 3.7 km (Fig. 1a) and inward with peak speeds of about 140 m/s near the flow head. With increasing time, the velocity peak flattens and becomes broader, and by t = 145 s, the maximum speed is about 75 m/s, decreasing gradually outward to 60 m/s at the flow head at a range of 6 km. Figure 1b shows that maximum values of P_{dyn} (about 12 kPa or 0.12 bar) occur at intermediate times and locations about 1 km behind the pyroclastic flow head. More typical values produced by this eruption, however, are about 6 kPa. Ash temperature ranges between 400 and 600 K (Fig. 1c); maximum values occur near the eruption column and decay gradually as radial distance increases. Figure 1d reveals laterally continuous solid volume fractions between 1×10^{-4} and 5×10^{-3} for later times. The head of the pyroclastic flow is shown to progress from a radial distance of 3.7 km to near 7 km during the 36 s of plotted times.

Figure 2 shows results from an eruption with conditions identical to the Figure 1 model, except the particle size has been increased to 2.0 cm (lapilli). Because the particles are coarser and have a higher settling velocity, the eruption fountain collapses from a height of only a few hundred metres. The collapsing part of the fountain hits the ground at about 500 m from vent center and moves radially outward as a pyroclastic flow. Figure 2a shows the evolution of horizontal flow velocity along the ground. An initially low-wavelength, high-amplitude velocity distribution with a maximum of 115 m/s at 2.9 km evolves to a broader spatial distribution as the pyroclastic flow moves outward. By t = 145 s, the maximum velocity has decreased to 45 m/s, and the front of the pyroclastic flow has reached a distance of 5.5 km. P_{dyn} shows a similar evolution

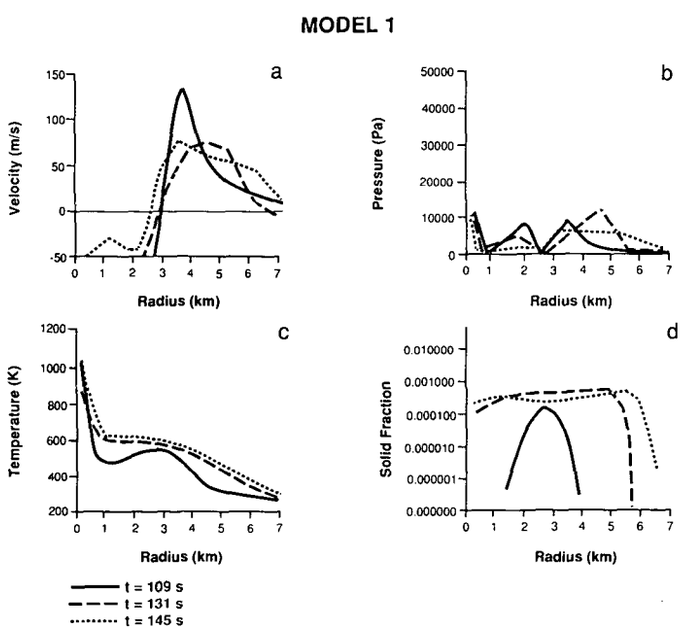

Figure 1. Pyroclastic flow properties as functions of distance from vent center. a: Horizontal velocity; b: horizontally directed dynamic pressure; c: temperature; d: particle volume fraction. Each parameter is shown for three times after initiation of discharge (t = 109, 131, and 145 s), earliest of which coincides with initial formation of pyroclastic flow. Eruption conditions are listed in Table 1.

(Fig. 2b), a maximum pressure of 52 kPa (5.2 bar) being present at early time decaying to 10 kPa at $t = 145$ s. Temperature decreases nearly linearly with distance to ambient (300 K; Fig. 2c). Solid volume fraction (Fig. 2d) shows a gradual decrease from 3×10^{-2} where the flow initially hits the ground to 2×10^{-3} at radial distances between 2 and 4 km. Near the head of the pyroclastic flow, θ shows a slight increase.

Eruption conditions similar to those calculated by Carey and Sigurdsson (1985) for the May 18, 1980, Plinian phase of Mount St. Helens were invoked for experimental results shown in Figure 3. An important difference between this model and the observed pyroclastic flows is that the latter initially flowed down a slope (the flank of the volcano), whereas the model flows move across a horizontal surface. Thus, the model runout distance is only about one-third of those observed at the volcano (approximately 9 km; Criswell, 1987), a consequence predicted by the energy-line model of Malin and Sheridan (1982). Figure 3a shows a similar evolution of velocity to that shown in Figure 2; an initial, sharp velocity peak of about 45 m/s flattens with time so that at $t = 200$ s the pyroclastic flow has an average velocity of about 10 m/s. Note the large negative velocities beyond 2.8 km, which correspond to ventward-directed atmospheric wind. Although this model eruption is relatively weak and produces a low pyroclastic fountain, some ash continues to rise above the vent because of buoyancy. The rising ash cloud attains vertical speeds of about 100 m/s and convectively draws atmosphere up with it. The resulting inward wind exerts enough drag to stagnate the pyroclastic flow. Dynamic pressure shows a sharp peak with a maximum of 1.4 kPa at intermediate time and range (Fig. 3b). The amplitude of the peak decreases with time, and the location of the peak migrates from initially near the flow head to more intermediate ranges, but its wavelength remains nearly constant because of the limited progress of the pyroclastic flow. Note that P_{dyn} increases again to about 0.2 kPa (at late times) beyond the pyroclastic flow due to a ventward-directed atmospheric wind of about 15 m/s. As with the previous two examples, temperature decreases smoothly with distance from vent (Fig. 3c). Solid volume fraction (Fig. 3d) in the pyroclastic flow increases with time to about 10^{-3} as ash accumulates, but the flow does not travel beyond 3 km.

DISCUSSION AND SUMMARY

Of the four variables plotted in Figures 1, 2, and 3, the best by which to predict structural damage is dynamic pressure. We note that atmospheric winds (particle-free) create dynamic pressures of 0.1 kPa, 1.0 kPa, and 10 kPa for wind speeds of 33 km/h, 105 km/h, and 334 km/h, respectively, for sea-level air density (1.16 kg/m^3). Thus, damage predicted by these model pyroclastic flows exceeds that expected for even the most violent of hurricanes and tornadoes under some conditions.

As shown above, the history of dynamic pressure at a given distance from vent can be quite complex, even though the eruptions have steady discharge rates for the duration of each experiment. For example, a structure at 3.6 km from vent of the eruption described in Figure 1 will first experience a dynamic pressure of 8 kPa, followed by a decrease to 4 kPa, and finally by an increase to about 7 kPa. A structure at 5 km distance from the same eruption will simultaneously experience a small P_{dyn}, directed toward the vent, followed by a reversal to 12 kPa, directed away from the vent, that gradually decreases to about 5.5 kPa. One can also imagine the complexity of erosion/deposition at a given location. The substrate at 3.6 km in the above eruption is eroded prior to tephra deposition; the deposits themselves are subsequently eroded. At 5 km from the vent an opposite sequence of deposition, erosion, and finally deposition should produce a depositional facies distinct from the near-vent location.

For the low pyroclastic fountain described by Figure 2, P_{dyn} goes through a simpler history for locations away from the vent. P_{dyn} goes through an initial sharp rise to 50 kPa at 3.6 km and 10 kPa at 5 km, followed by a gradual decrease with time that is less pronounced at greater distances. The greater damage potential of this eruption is the result of much denser pyroclastic flow than that described by Figure 1; the coarser

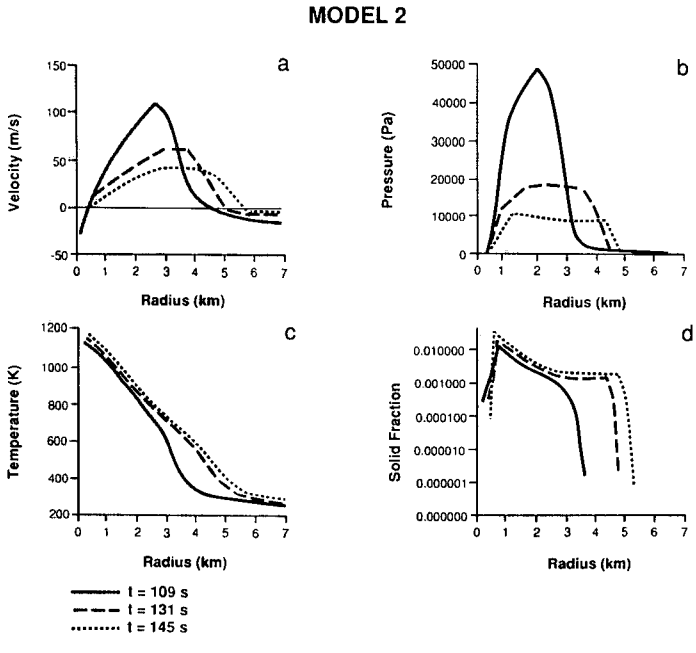

Figure 2. Plots of pyroclastic flow parameters as functions of distance from vent as in Figure 1. Plot times and eruption conditions are identical to those of Figure 1 except for larger particle size (Table 1).

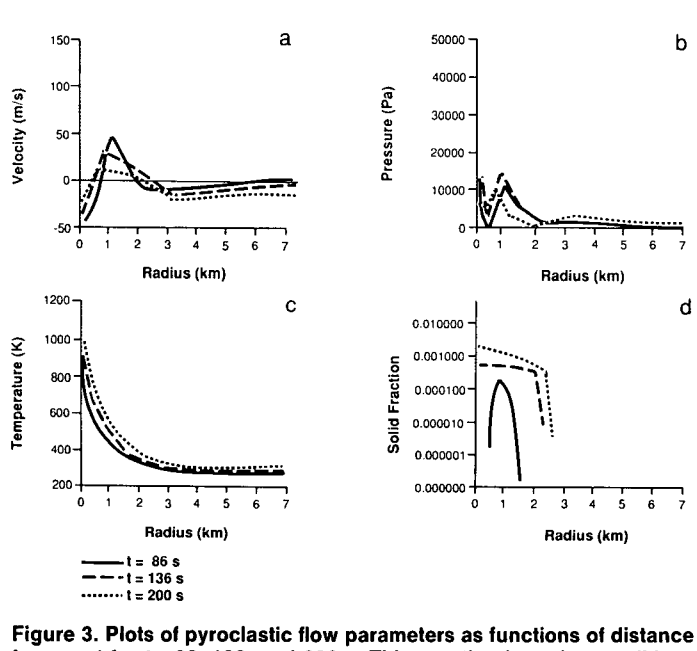

Figure 3. Plots of pyroclastic flow parameters as functions of distance from vent for $t = 86$, 136, and 200 s. This eruption is under conditions (Table 1) that might be expected for typical Plinian eruption from stratovolcano, and has similar conditions to those estimated by Carey and Sigurdsson (1985) for May 18, 1980, Plinian eruption of Mount St. Helens.

clasts in Figure 2 settle to the bottom of the flow much faster than the finer clasts in the Figure 1 eruption.

By comparison, Figure 3 describes an eruption that produces a weak pyroclastic flow whose runout is only a few kilometres. The dynamic pressures reach modest peaks of about 1 kPa within the flow, and smaller pressures (about 0.2 kPa), which are directed toward the vent, exist just beyond the outer margin of the flow. Figure 3c records an initially dilute pyroclastic flow that becomes denser and slows with time.

Figures 1, 2, and 3 demonstrate that pyroclastic flows tend to have two maxima in solid volume fraction. The first of these occurs at the point where the pyroclastic fountains initially hit the ground. The second is in the head region of the flows. This second maximum also corresponds to a maximum horizontal velocity; thus, the highest mass flux of tephra at any given time in pyroclastic flow evolution (outside the near-vent high-concentration region) occurs in the head of the flow.

Numerical modeling of explosive eruptions provides much insight into the complex processes associated with pyroclastic flows. From the modeling it is possible to approximate environmental effects of the flows that are of value to volcanic hazards assessment and to interpretation of deposits from pyroclastic flows. As multiphase flow theory advances and computational power increases, we expect that modeling will approach the complexity of natural eruptions and more complete assessments of pyroclastic transport processes will be possible.

REFERENCES CITED

Beget, J.E., and Limke, A.J., 1988, Two-dimensional kinematic and rheological modeling of the 1912 pyroclastic flow, Katmai, Alaska: Bulletin of Volcanology, v. 50, p. 148–160.

Carey, S., and Sigurdsson, H., 1985, The May 18, 1980, eruption of Mount St. Helens; 2. Modeling of dynamics of the Plinian phase: Journal of Geophysical Research, v. 90, p. 2948–2958.

——1986, The 1982 eruptions of El Chichon volcano, Mexico (2): Observations and numerical modeling of tephra-fall distribution: Bulletin of Volcanology, v. 48, p. 127–142.

——1987, Temporal variations in column height and magma discharge rate during the 79 A.D. eruption of Vesuvius: Geological Society of America Bulletin, v. 99, p. 303–314.

Carey, S., and Sparks, R.S.J., 1986, Quantitative models of the fallout and dispersal of tephra from volcanic eruption columns: Bulletin of Volcanology, v. 48, p. 109–126.

Crandell, D.R., and Hoblitt, R.P., 1986, Lateral blasts at Mount St. Helens and hazard zonation: Bulletin of Volcanology, v. 48, p. 27–37.

Criswell, C.W., 1987, Chronology and pyroclastic stratigraphy of the May 18, 1980, eruption of Mount St. Helens, Washington: Journal of Geophysical Research, v. 92, p. 10237–10266.

Freundt, A., and Schmincke, H.-U., 1986, Emplacement of small-volume pyroclastic flows at Laacher See (East-Eifel, Germany): Bulletin of Volcanology, v. 48, p. 39–60.

Harlow, F.H., and Amsden, A.A., 1975, Numerical calculation of multiphase fluid flow: Journal of Computational Physics, v. 17, p. 19–52.

Kieffer, S.W., 1981, Fluid dynamics of the May 18 blast at Mount St. Helens: U.S. Geological Survey Professional Paper 1250, p. 379–400.

Malin, M.C., and Sheridan, M.F., 1982, Computer-assisted mapping of pyroclastic surges: Science, v. 217, p. 637–640.

Sheridan, M.F., 1979, Emplacement of pyroclastic flows: A review, *in* Chapin, C.E., and Elston, W.E., eds., Ash flow tuffs: Geological Society of America Special Paper 180, p. 125–136.

Siebert, L., Glicken, H., and Ui, T., 1987, Volcanic hazards from Bezymianny- and Bandai-type eruptions: Bulletin of Volcanology, v. 49, p. 435–459.

Sigurdsson, H., Carey, S., Cornell, W., and Pescatore, T., 1985, The eruption of Vesuvius in A.D. 79: National Geographic Research, v. 1, p. 332–387.

Sigurdsson, H., Carey, S., and Fisher, R.V., 1987, The 1982 eruption of El Chichon volcano, Mexico (3): Physical properties of pyroclastic surges: Bulletin of Volcanology, v. 49, p. 467–488.

Sparks, R.S.J., 1976, Grain size variations in ignimbrites and implications for the transport of pyroclastic flows: Sedimentology, v. 23, p. 147–188.

——1986, The dimensions and dynamics of volcanic eruption columns: Bulletin of Volcanology, v. 48, p. 3–16.

Sparks, R.S.J., and Wilson, L., 1982, Explosive volcanic eruptions—V. Observations of plume dynamics during the 1979 Soufriere eruption, St. Vincent: Royal Astronomical Society Geophysical Journal, v. 69, p. 551–570.

Valentine, G.A., 1987, Stratified flow in pyroclastic surges: Bulletin of Volcanology, v. 49, p. 616–630.

Valentine, G.A., and Fisher, R.V., 1986, Origin of layer 1 deposits in ignimbrites: Geology, v. 14, p. 146–148.

Valentine, G.A., and Wohletz, K.H., 1989, Numerical models of Plinian eruption columns and pyroclastic flows: Journal of Geophysical Research, v. 94, p. 1867–1887.

Wilson, C.J.N., 1980, The role of fluidization in the emplacement of pyroclastic flows: An experimental approach: Journal of Volcanology and Geothermal Research, v. 8, p. 231–249.

——1984, The role of fluidization in the emplacement of pyroclastic flows, 2: Experimental results and their interpretation: Journal of Volcanology and Geothermal Research, v. 20, p. 55–84.

——1985, The Taupo eruption, New Zealand II. The Taupo ignimbrites: Royal Society of London Philosophical Transactions, ser. A, v. 314, p. 229–310.

Wilson, L., 1976, Explosive volcanic eruptions—III. Plinian eruption columns: Royal Astronomical Society Geophysical Journal, v. 45, p. 543–556.

Wilson, L., and Walker, G.P.L., 1987, Explosive volcanic eruptions—VI. Ejecta dispersal in Plinian eruptions: The control of eruption conditions and atmospheric properties: Royal Astronomical Society Geophysical Journal, v. 89, p. 657–679.

Wilson, L., Sparks, R.S.J., Huang, T.C., and Watkins, N.D., 1978, The control of volcanic eruption column heights by eruption energetics and dynamics: Journal of Geophysical Research, v. 83, p. 1829–1836.

Wilson, L., Sparks, R.S.J., and Walker, G.P.L., 1980, Explosive volcanic eruptions—IV. The control of magma properties and conduit geometry on eruption column behavior: Royal Astronomical Society Geophysical Journal, v. 63, p. 117–148.

Wohletz, K.H., and Sheridan, M.F., 1979, A model of pyroclastic surge, *in* Chapin, C.E., and Elston, W.E., eds., Ash flow tuffs: Geological Society of America Special Paper 180, p. 177–194.

Wohletz, K.H., McGetchin, T.R., Sandford, M.T., II, and Jones, E.M., 1984, Hydrodynamic aspects of caldera-forming eruptions; numerical models, *in* Calderas and associated igneous rocks: Journal of Geophysical Research, v. 89, p. 8269–8285.

Woods, A.W., 1988, The fluid dynamics and thermodynamics of eruption columns: Bulletin of Volcanology, v. 50, p. 169–193.

ACKNOWLEDGMENTS

Funded by Institutional Supported Research and Development funds (U.S. Department of Energy) at Los Alamos National Laboratory. We thank Rodney Whitaker for a helpful review of the manuscript and Marty Horn for his adaptation of the computer code used herein for applications to volcanic problems.

Manuscript received September 2, 1988
Revised manuscript received March 16, 1989
Manuscript accepted April 6, 1989